

Monitoring precipitable water vapor in real-time using global navigation satellite systems

Seung-Woo Lee · Jan Kouba · Bob Schutz ·
Do Hyeong Kim · Young Jae Lee

Received: 11 March 2013 / Accepted: 30 July 2013 / Published online: 11 August 2013
© Springer-Verlag Berlin Heidelberg 2013

Abstract This paper addresses real-time monitoring of the precipitable water vapor (PWV) from GNSS measurements and presents some results obtained from 6-month long GNSS PWV experiments using international and domestic GNSS networks. In the real-time GNSS PWV monitoring system a server/client structure is employed to facilitate formation of PWV networks and single-differenced GNSS measurements are utilized to mitigate errors in GNSS satellites' orbits and clocks. An issue relating to baseline length between the server and clients is discussed in detail and as a result the PWV monitor is configured to perform in two modes depending on the baseline length. The server estimates sequentially the zenith wet delay of the individual stations, which is then converted into the PWV of the stations. We evaluate system performance by comparing the real-time PWV solution with reference solutions including meteorological measurements obtained with radiosondes and deferred-time preci-

sion GNSS PWV solutions. Results showed that the standard deviation of difference between the real-time PWV and the reference solutions ranged from 2.1 to 3.4 mm in PWV for a 6-month long comparison, which was improved to 1.4 to 2.9 mm by reducing comparison period to 20 days in winter.

Keywords GNSS · Precipitable water vapor (PWV) · Real-time

1 Introduction

The Earth's troposphere is one of influential error sources which can limit performance of the Global Navigation Satellite Systems (GNSS). The signal delay due to the troposphere becomes a critical issue, especially for precision GNSS applications including nanosecond-level time transfer (Lee et al. 2008; Lee and Kim 2009). Compared with the ionospheric delay which arises also due to existence of the Earth's atmosphere, the ionospheric delay is mostly cancelled out by use of the dual-frequency GNSS measurements while the tropospheric delay is more difficult to mitigate, particularly the wet component of the delay. This is mainly due to high variability in temporal and spatial distribution of the atmospheric water vapor that is responsible for the wet delay.

While mitigation of the tropospheric delay directly benefits many precision GNSS applications, the tropospheric wet delay has in itself an important physical meaning in meteorology. This is due to the fact that the tropospheric wet delay is well correlated to the quantity of water vapor integrated along the signal path. As a result, the wet delay estimate from GNSS measurements can be used to quantify the atmospheric water vapor or the precipitable water vapor (PWV).

PWV is one of important quantities in meteorology because the atmospheric water vapor plays a key role in the

S.-W. Lee (✉)

Pusan National University, Busandaehak-ro 63 beon-gil
Geumjeong-gu, Busan 609-735, South Korea
e-mail: leeseungwoo@hotmail.com

J. Kouba

Geodetic Survey Division, Natural Resources Canada, 615 Booth
Str, Ottawa, ON K1A 0E9, Canada

B. Schutz

Department of Aerospace Engineering and Engineering
Mechanics, The University of Texas at Austin,
Austin, TX 78712, USA

D. H. Kim

National Meteorological Satellite Center, Korea Meteorological
Administration, Seoul, South Korea

Y. J. Lee

Aerospace Information Engineering, Konkuk University,
1 Hwayang-dong, Gwangjin-gu, Seoul 143-701, South Korea

Earth's climate system. In addition water vapor is one of greenhouse gases and is expected to increase as global warming proceeds. A better knowledge of its distribution benefits various meteorological researches ranging from regional and global climate research, numerical weather prediction (Haan and Barlag 2002; Gendt et al. 2004) to global warming monitor (Stevens 1999; Gutman et al. 2004). However, the atmospheric water vapor has been often one of the most poorly characterized quantities in practice. Meteorologists have used several sensors and platforms to measure the atmospheric water vapor including the radiosonde and the Microwave Radiometer (MWR). Each instrument has its own strengths and weaknesses and for example a radiosonde or weather balloon can make direct, in-situ measurements of air temperature, humidity and pressure at varying altitudes which can reach up to 30 km. This suggests that good vertical resolution can be achieved with the radiosonde while it may suffer from poor horizontal and temporal resolutions, taking into account the fact that radiosonde is typically restricted to be launched every 12 or 24 h a day due to cost considerations, that is, it is hardly reusable. The ground-based MWR, on the other hand, has good temporal resolution but it should be tuned to site-dependent conditions and is weather-sensitive, that is, it does not work properly in rainy or heavily foggy conditions.

Compared with these traditional platforms, GNSS can provide several advantages including practically no operating expense, all-weather operability and good spatial (and temporal) coverage. Such coverage of GNSS is partly because the GNSS stations are distributed much more densely over the world than meteorological observatories. Motivated by the advantages, it has been demonstrated that GNSS could provide accurate estimates that are comparable to the measurements by traditional PWV sensors. Bevis et al. (1992) showed that the GPS sensed PWV estimates obtained in deferred-time mode agreed with MWR measurements within the level of 2 mm in RMS and that the mean between the two PWV results was typically less than 2 mm. Rocken et al. (1997) demonstrated that the GPS PWV estimate could be retrieved in the Near Real-Time (NRT) mode and the performance of the GPS PWV in the NRT mode was evaluated by comparing against the radiosonde measurements based on 4-month long GPS data, where the RMS difference between the GPS PWV and radiosonde measurements was found to be within 2.1 mm. In the NRT mode, latency was reported to be within 30 min after data collection. Ware et al. (2000) introduced a real-time GPS network for atmospheric research, named as the Suominet, where real-time worldwide communication links were established for GPS data transfer and output distribution. In Suominet, every 1-h batch of GPS data is processed with the Bernese S/W package to produce PWV estimates and accordingly the PWV results are updated on a hourly basis. Karabatic et al. (2011) examined the perfor-

mance of the NRT PWV estimation technique to assist the numerical weather prediction (NWP) in Austria and analysed the effects of some parameters on the PWV estimation such as the GNSS ephemeris. The GNSS-derived PWV was computed with Bernese software with a latency of 1 h, and it was reported to agree with radiosonde-derived PWV within 2 mm in an RMS sense. The precision point positioning (PPP) technique was also examined as a possible alternative to the conventional double-difference approach.

A notable example of the application of the GNSS PWV technique to operational meteorology is with E-GVAP (<http://egvap.dmi.dk/>). The E-GVAP is intended to further the outcomes of the COST Action 716, which is a European research project on the meteorological use of the GNSS-derived PWV (Elgered et al. 2005). In the E-GVAP, more than 1,500 ground GNSS sites are utilized to form a ground-based GNSS tracking network and the network data are processed in near real-time to estimate PWV for use in the data assimilation process in NWP and in now-casting to the participating EUMETNET members. Also, the NRT GNSS PWV monitoring for numerical weather prediction is currently operational in Germany (Heise et al. 2009).

While the above activities are based on near real-time estimation of PWV, there are some other works on real-time PWV estimation where processing delay is typically at the level of a few seconds or less. Hernandez-Pajares et al. (2001) presented a real-time PWV estimation strategy based on the Wide Area Differential GPS (WADGPS) network. According to the strategy, PWV estimates are computed every 5 min with the double-difference Kalman filter and ionospheric tomography. They compared the ZTD estimates with the IGS final tropospheric estimates, and the RMS difference in ZTD between the solutions was reported to be about 1.0–1.4 cm (1.5–2.1 mm in PWV) during the 4-day long comparison. Note that their comparison is basically an intra-technique comparison, i.e. comparison between a GNSS-derived ZTD solution with another GNSS-derived ZTD rather than with solutions that are independent of the GNSS technique. Iwabuchi et al. (2006, 2011) showed that real-time PWV estimation could be achieved either with double-differenced or un-differenced approach. Unlike Karabatic et al. (2011), their PPP approach is based on the IGS Ultra-rapid orbit and a custom satellite clock estimator. The use of their own clock estimator is due to the fact that the accuracy of the (predicted) IGS Ultra-rapid clock is considerably poorer than its orbit counterpart. The level of agreement between GNSS-derived PWV and radiosonde PWV was reported to be 2.4 mm for the double-difference approach and 3.8 mm for the PPP approach.

In summary, (near) real-time GNSS PWV estimation has been performed either by the network approach using double-difference measurements (Rocken et al. 1997; Hernandez-Pajares et al. 2001; Iwabuchi et al. 2006; Karabatic et al.

2011) or the PPP approach using un-difference measurements (Iwabuchi et al. 2006; Karabatic et al. 2011). While the PPP approach has proven to be effective in the deferred-time mode (Byun and Bar-Server 2009; Karabatic et al. 2011), the approach is difficult to use in real-time applications because a precise ephemeris like the IGS Final ephemeris is generally unavailable in real-time. In contrast, the double-difference approach has been successfully used in (near) real-time applications. This is mainly because the satellite clock errors (and some portion of orbit errors too) can be effectively cancelled out during the double-differencing process. However, the double-difference approach requires more computations and bookkeeping processes compared with the PPP approach. Furthermore, processing all network data with the double-difference approach can be time-consuming, particularly as the number of stations becomes greater, for example, a few hundred or more. This is due to the fact that the number of computations required in the network approach tends to grow parabolically rather than linearly with increments of the number of stations.

The goal of the study was to develop a truly real-time GNSS PWV estimation technique for meteorological purposes such as rapid delivery of humidity information for numerical weather now-casting and forecasting. We propose the use of a baseline-by-baseline processing scheme based on single-differenced GNSS measurements. Compared with the conventional PPP and double-difference approaches, the single-difference approach has the same advantage of cancelling out the satellite clock errors as the network approach while the number of computations increases linearly rather than parabolically with the increment of the number of stations in our approach. However, the single-difference approach still requires the estimation of the clock difference between stations, which is similar to the PPP approach. In addition, we addressed the issue of a filter divergence that can happen in local GNSS PWV networks where the individual stations are rather densely distributed and, thus, not separated by a sufficient distance, that is, about 500 km.

We describe a real-time technique to monitor PWV from GNSS measurements and emphasis is placed on immediate retrieval of PWV. Section 2 presents the basic formulation and implementation of the GNSS PWV monitoring system together with an analysis on the filter divergence caused by insufficient separation between stations. Section 3 shows results obtained by processing 6-month long GNSS data from international and domestic GNSS networks. Performance evaluation of the system is conducted by comparing real-time PWV solution with radiosonde PWV measurements and another precision GNSS PWV solution computed by the GIPSY OASIS II software package. Section 4 presents our conclusions.

2 Formulation and system implementation

The working GNSS signal used in the study is the single-differenced (SD), ionosphere-free or L3 carrier phase measurement, which is the same type of measurement that is used in the carrier-phase common-view GNSS time transfer. The main reason for using SD measurements instead of un-differenced (UD) measurements is to cancel out the satellite clock and orbit errors in real-time. For more detailed description on the SD measurement, readers are referred to (Lee and Kim 2009).

Let us assume two GNSS stations A and B view a common satellite S. Then SD pseudorange and carrier-phase measurements can be expressed as

$$\begin{aligned}\Psi_{AB} &= \Psi_A - \Psi_B = \rho_{AB}^S + c\delta_{AB} + T_{AB}^S + m_{\psi,AB}^S + \varepsilon_{\psi,AB} \\ \Phi_{AB} &= \Phi_A - \Phi_B = \rho_{AB}^S + c\delta_{AB} + N_{AB}^S \lambda_{L3} + T_{AB}^S \\ &\quad + m_{\phi,AB}^S + \varepsilon_{\phi,AB}\end{aligned}\quad (1)$$

In Eq. 1 superscript S denotes the common satellite and subscript A and B denote the ground stations. The terms in Eq. 1 denote SD geometric range (ρ_{AB}^S), SD clock bias or time difference between the stations (δ_{AB}) multiplied by the speed of light (c), SD tropospheric delay (T_{AB}^S), respectively. While the magnitude of these terms is the same in both pseudorange and carrier-phase measurements, the other terms depends on the type of the GNSS measurements, which include L3 phase ambiguity (N_{AB}^S) multiplied by L3 wavelength (λ_{L3}), SD pseudo-range multi-path error ($m_{\psi,AB}^S$), SD carrier-phase multi-path error ($m_{\phi,AB}^S$), SD pseudo-range measurement noise ($\varepsilon_{\psi,AB}$) and SD carrier-phase measurement noise ($\varepsilon_{\phi,AB}$). The important term in the GNSS PWV problem is T_{AB}^S , which is expressed in terms of two UD tropospheric delays:

$$T_{AB}^S = T_A^S - T_B^S \quad (2)$$

Furthermore, each UD tropospheric delay (T_A^S and T_B^S) can be divided into two components: hydrostatic delay and wet delay. Hydrostatic delay is generally predictable and can be removed using models, but wet delay is highly variable and should be estimated. For a given elevation angle of S , the two delay components can be expressed by a product of the delay in the receiver's zenith direction (elevation angle of 90°) and elevation-dependent mapping function. Accordingly the UD tropospheric delay can be expressed as

$$\begin{aligned}T_R^S &= T_h^S + T_w^S = m_{fh}z_h + m_{fw}z_w + \frac{\partial m_{fw}}{\partial z_w} \cos Az_R^S \cdot g^n \\ &\quad + \frac{\partial m_{fw}}{\partial z_w} \sin Az_R^S \cdot g^e\end{aligned}\quad (3)$$

In Eq. 3 subscript R represents either A or B . m_{fh} , m_{fw} , z_h and z_w denote in sequence tropospheric hydrostatic mapping

function, tropospheric wet mapping function, Zenith Hydrostatic Delay (ZHD) and Zenith Wet Delay (ZWD). The sum of ZHD and ZWD is called the Zenith Total Delay (ZTD). The last two terms in Eq. 3 are introduced for accommodating the azimuthal dependency of the tropospheric delay (Bar-Server et al. 1998) and Az_R^S , g^e and g^n denote the azimuth angle, gradient parameter in east-west direction and gradient parameter in north-south direction, respectively.

It is ZWD that is related to PWV. To estimate the ZWD of two stations from SD measurements is possible only if the wet mapping functions of the two stations, denoted as $mf_{A,w}$ and $mf_{B,w}$, are sufficiently different from each other. If $mf_{A,w}$ and $mf_{B,w}$ are close or have the same value, say mf_w , then the SD ZWD equation is reduced to

$$mf_{A,w}z_{A,w} - mf_{B,w}z_{B,w} \approx mf_w (z_{A,w} - z_{B,w}) \tag{4}$$

Equation 4 implies that only difference in ZWD between the two stations can be estimated in such case. Taking into account that the mapping functions typically depend on station location as well as satellite elevation angle, the stations located nearby each other are likely to have the similar mapping functions. The minimum baseline length to avoid these conditions has not been verified clearly yet but as a rule of thumb, the baseline length of more than 500 km is generally thought to be sufficient. For a station pair whose baseline length is less than the minimum requirement, say 500 km, one ZWD needs to be fixed to the value that is determined a priori, for example, by other techniques. That way the other ZWD is computed relatively, that is, by using the estimated difference in ZWDs and the fixed ZWD. Otherwise, forcing estimation of both ZWDs for the station pair that is not sufficiently separated apart leads to the filter divergence, where the estimated ZWD values become divergent and meaningless. This situation is basically the same as that of solving a set of under-determined algebraic equations, where there exist infinitely many possible solutions.

The above considerations lead to categorization of GNSS-based ZWD estimation into two modes: one is the absolute mode where stations are separated sufficiently from each other and thus ZWD of both stations can be estimated simultaneously. The other is relative mode where the stations are close to each other and one ZWD should be estimated with reference to the other ZWD that needs to be determined a priori.

Once both ZWDs are obtained either absolutely or relatively, the ZWD can be directly related to the PWV of the stations:

$$\text{ZWD} = \Pi \cdot \text{PWV} = \Pi \cdot \text{I WV} / \rho_w \tag{5}$$

where

$$\Pi = 10^{-6} [\rho_w R_v (k_2 + k_3 / T_m)] \approx 0.102 + 1,708.08 / T_m$$

In Eq. 5 IWV stands for the Integrated Water Vapor and is sometimes used as an alternative of PWV in meteorology. The relationship between PWV and IWV is obvious from Eq. 5. k_2 and k_3 are refractivity constants which are 22.1 K/hPa and 370,100 K²/hPa, respectively, and ρ_w , R_v and T_m denote in turn the density of water vapor, specific gas constant for water vapor, weighted mean temperature of the troposphere. The value of Π is typically around 0.15 and can be changed up to 15 % depending on the atmospheric mean temperature (T_m). T_m can be approximated by the surface (ground) temperature (T_0) of the individual stations. Bevis et al. (1992) provided an empirical relation between T_m and T_0 , which is expressed as

$$T_m = 70.2 + 0.72 \cdot T_0 \tag{6}$$

In our system, Eqs. 1–3, 5 and 6 are incorporated to a sequential data processor for the real-time GNSS-based PWV monitor. The extended Kalman filter (EKF) formulation is utilized for sequential estimation of PWV and for comprehensive description on the EKF formulation; readers are referred to Brown and Hwang (1997).

The implementation of EKF for the real-time PWV estimation is summarized as follows. Based on Eq. 1, the state vector at the k th epoch can be expressed in partitioned form as

$$\mathbf{x}(k) = \begin{bmatrix} \mathbf{x}_{\text{pos}} \\ \mathbf{x}_{\text{clk}} \\ \mathbf{x}_{\text{tro}} \\ \mathbf{x}_{\text{amb}} \end{bmatrix}_k \tag{7}$$

Each partitioned component of the state vector corresponds to the terms in Eq. 1, that is, \mathbf{x}_{pos} to ρ_{AB}^S , \mathbf{x}_{clk} to δt_{AB} , \mathbf{x}_{tro} to T_{AB}^S and \mathbf{x}_{amb} to $N_{AB}^S \lambda_{L3}$. Provided that the number of visible satellites is N_k at the k th epoch, these vectors can be given as follows:

$$\mathbf{x}_{\text{pos}} = \begin{bmatrix} x_B \\ y_B \\ z_B \end{bmatrix} \quad \mathbf{x}_{\text{clk}} = [\delta t_{AB}] \quad \mathbf{x}_{\text{tro}} = \begin{bmatrix} zw_A \\ gn_A \\ ge_A \\ zw_B \\ gn_B \\ ge_B \end{bmatrix}$$

$$\mathbf{x}_{\text{amb}} = \begin{bmatrix} b_1 \\ b_2 \\ \vdots \\ b_{N_k} \end{bmatrix} \tag{8}$$

In Eq. 8 x_B , y_B and z_B denote the Cartesian coordinates of the client station B . Our method uses the single-differenced GNSS measurements, which is essentially relative positioning and the position of one of the stations needs to be fixed in space. This is why the position of A (the server) is fixed to a priori values. δt_{AB} represents the time difference between

the clocks of A and B . z_{w_A} , g_{n_A} , and g_{e_A} represent the tropospheric zenith wet delay and the corresponding northern and eastern zenith gradient parameters of A , respectively, and the same state variables are repeatedly assigned for B . Finally, b_j denotes the phase ambiguity of the j th satellite. According to Eq. 8, $\mathbf{x}(k)$ is an $(N_k + 10) \times 1$ column vector.

In the GPS PWV estimation, the quantity of greatest interest is \mathbf{x}_{tro} , and it is typically modeled as a random walk vector. If \mathbf{x}_{tro} evolves from t_k to t_{k+1} , the discrete formulation of \mathbf{x}_{tro} can be given as follows:

$$\mathbf{x}_{\text{tro},k+1} = \mathbf{x}_{\text{tro},k} + \mathbf{q}_k \tag{9}$$

where

$$E[\mathbf{q}_k \mathbf{q}_k^T] = \mathbf{Q}_k \\ = \text{diag}[q_{w_A} \Delta t \ q_{g_{n_A}} \Delta t \ q_{g_{e_A}} \Delta t \ q_{w_B} \Delta t \ q_{g_{n_B}} \Delta t \ q_{g_{e_B}} \Delta t]$$

$$\Delta t = t_{k+1} - t_k$$

In Eq. 9, E denotes the expectation operation and diag means diagonal entries for a square matrix whose off-diagonal entries are all zeroes. As shown in Eq. 8, \mathbf{x}_{tro} is 6×1 column vector and \mathbf{Q}_k becomes 6×6 square matrix. \mathbf{q}_k is a random vector whose intensity is used to define the process noise covariance of \mathbf{x}_{tro} , as given in Eq. 9. q_{w_A} , $q_{g_{n_A}}$, and $q_{g_{e_A}}$ denote the noise intensity of the tropospheric zenith wet delay and associated northern and eastern horizontal gradients for station A , respectively, and similar quantities are again assigned for station B .

Recalling Eq. 1, any errors in station coordinates or tropospheric parameters will degrade the accuracy of the filter estimates. While estimating the tropospheric parameters is a linear estimation problem, estimating the client station's coordinates is a nonlinear estimation problem due to the nonlinear relation between receiver position and the GNSS measurement. Generally, nonlinear estimation problems should be solved with nonlinear techniques including the recursive least square method, the EKF, and the particle filter. The nonlinearity of the GNSS PWV problem exists only in the observation equation (or measurement dynamics) and not in the system dynamics, and most parts of the EKF formulation for the GNSS PWV problem are the same as the Kalman filter that is designed for solving linear problems. The EKF formulation can be summarized as follows:

$$\tilde{\mathbf{x}}(k) = \Phi(k) \hat{\mathbf{x}}(k-1) \tag{10}$$

$$\tilde{\mathbf{P}}(k) = \Phi(k) \hat{\mathbf{P}}(k-1) \Phi^T(k) + \mathbf{Q} \tag{11}$$

$$\mathbf{K}(k) = \tilde{\mathbf{P}}(k) \mathbf{H}^T(\tilde{\mathbf{x}}(k)) \\ \left[\mathbf{H}(\tilde{\mathbf{x}}(k)) \tilde{\mathbf{P}}(k) \mathbf{H}^T(\tilde{\mathbf{x}}(k)) + \mathbf{R} \right]^{-1} \tag{12}$$

$$\hat{\mathbf{x}}(k) = \tilde{\mathbf{x}}(k) + \mathbf{K}(k) (\mathbf{z}(k) - \mathbf{h}(k) (\tilde{\mathbf{x}}(k))) \tag{13}$$

$$\hat{\mathbf{P}}(k) = (\mathbf{I} - \mathbf{K}(k) \mathbf{H}(\tilde{\mathbf{x}}(k))) \tilde{\mathbf{P}}(k). \tag{14}$$

In Eqs. 10–14, the terms with tildes represent quantities obtained by prediction and the terms with carats represent quantities obtained by measurement update. \mathbf{P} , \mathbf{Q} , \mathbf{R} , \mathbf{K} , and Φ are estimation error covariance, process noise covariance, measurement noise covariance, Kalman gain and state transition matrix, respectively. \mathbf{H} and \mathbf{h} denote the design matrix and measurement dynamics, respectively, and \mathbf{H} is computed repeatedly by evaluating the derivative of \mathbf{h} with respect to \mathbf{x} with the predicted values at the k th epoch. The main difference in the above formation from the Kalman filter lies in Eq. 13, where the innovation process is computed from the measurement dynamics itself, not in terms of its derivative \mathbf{H} . The above formulation is used in implementing a real-time PWV monitor system.

Once a real-time PWV monitor is set up for two stations (single baseline), it can be readily expanded to more than two stations (multiple baselines) in the server/client structure simply by processing the individual baselines one after another, which results in a PWV monitor network. Figure 1 shows a schematic of the real-time PWV monitoring system.

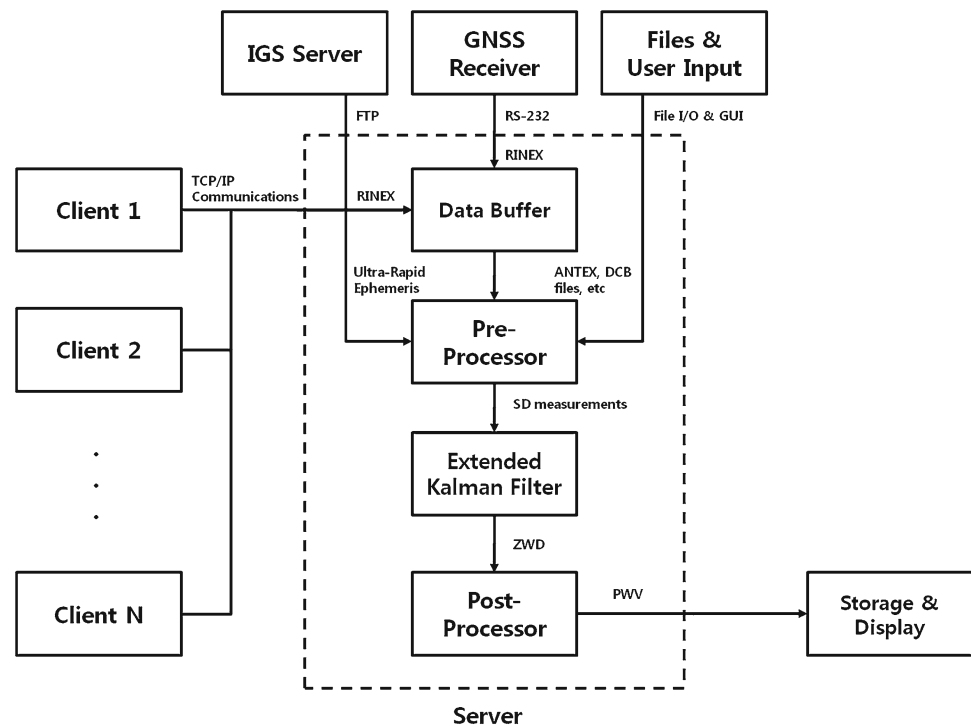
3 Results and discussion

The real-time system described in the previous section was tested by performing actual PWV monitoring with international and domestic GNSS networks. However, real-time data transfer links have not been established yet and alternatively a data playback module was utilized to transfer the GNSS data via TCP/IP communications. This enables the data transfer in the same manner as real-time case. In the data playback module the GNSS RINEX files are parsed and the code and carrier-phase data together with other necessary information including station designator and time tag are extracted and packaged into the TCP protocol. The module finally sends data packets to the server with a user-specified latency. Except for the data playback module, the rest of the system is the same as the real-time case.

Taking into account the effects of baseline length on PWV estimation, two different GNSS networks were set up: international and domestic networks. The international network consists of three GNSS stations from China, Japan and Korea and the domestic network is comprised of four Korean stations. In choosing member stations of the network, priority is given to the aspect irrespective of whether there exist nearby meteorological observatories or not. This is for the availability of independent PWV measurements from meteorological sensors such as Radiosonde (RS), which can serve as the ground truth for the real-time GNSS PWV solution.

Recalling Eqs. 1 and 3, the parameters estimated by the sequential filter include the Cartesian coordinates of the clients, time difference between the server and clients, float phase ambiguity, east-west and south-north gradient

Fig. 1 Schematic of real-time PWV monitoring system



parameters of the clients as well as ZWD of the clients. The location and two gradient parameters of the server are not estimated to enhance numerical stability. Mapping from slant tropospheric delay to zenith tropospheric delay is conducted using the global mapping function (GMF) (Böhm et al. 2006; Kouba 2008). Note that only the GPS constellation was used for the study. This is partly because the other GNSS constellations including the Galileo system were not fully operational at the time of conducting the study.

3.1 International PWV monitor network

Three GNSS stations from Japan, China and Korea were chosen for the international network, whose station designators are AIRA, SHAO and SUWN, respectively. AIRA has a nearby meteorological observatory that is located in Kagoshima, Japan and SHAO has a matching meteorological station located in Shanghai, China. The SUWN station in Korea is configured to be the server and has a matching meteorological observatory in Osan, Korea. Figure 2 shows the geographical location of the GNSS stations. The baseline lengths of the SUWN–AIRA and SUWN–SHAO links are 686 and 871 km, 4. As mentioned in Sect. 2, the absolute PWV estimation requires two stations to be apart by a sufficient distance, say 500 km, and the international network suffices the condition. Table 1 shows the geographic location of the GNSS stations and radiosonde observatories used in the experiments, which is expressed in terms of latitude, longitude and ellipsoidal height.

Because the AIRA, SHAO, and SUWN stations also belong to the global International GNSS Service (IGS) network, ZTD solutions of these stations have been continuously provided by IGS on a daily basis. During the PWV monitor experiments, the IGS ZTD solution had been computed with the GOA II (Byun and Bar-Server 2009). It is noted that the IGS Final Tropospheric Estimates dated 2011/04/17 or later are produced by USNO with Bernese software (Byram et al. 2011; Byram and Hackman 2012).

To obtain the PWV from the IGS ZTD solution, the value of ZHD should be known so as to be subtracted from the ZTD. The ZHD model used in the experiments is that given by Saastamoinen (1972), which is also the model implemented in the real-time filter.

$$\text{ZHD} = \frac{0.0022768p}{1 - 0.00266 \cos(2\phi) - 2.8 \times 10^{-7} h} \quad (15)$$

In Eq. 15, p represents the surface pressure in millibars at the site whose latitude and height are ϕ in radians and h in meters, respectively.

Recalling Eq. 9, the values of the covariance rate for random walk processes need to be determined to run the filter, and q_w , q_{gn} , and q_{ge} were set to $1.4 \times 10^{-8} \text{ m}^2/\text{s}$, $6.9 \times 10^{-10} \text{ m}^2/\text{s}$, and $6.9 \times 10^{-10} \text{ m}^2/\text{s}$, respectively. The value of q_w is translated to approximately $7 \text{ mm/h}^{1/2}$, which is comparable to the mean noise intensity of $4.8 \text{ mm/h}^{1/2}$ for the IGS stations given by Schueler et al. (2000).

The IGS Ultra-rapid ephemeris was used in the experiments, which is the only ephemeris available in real-time in the IGS product suite. Since the predicted clock of the IGS

Fig. 2 Geographical location of GNSS stations used in the study; the *solid squares* represent the international network and the *solid triangles* the domestic network

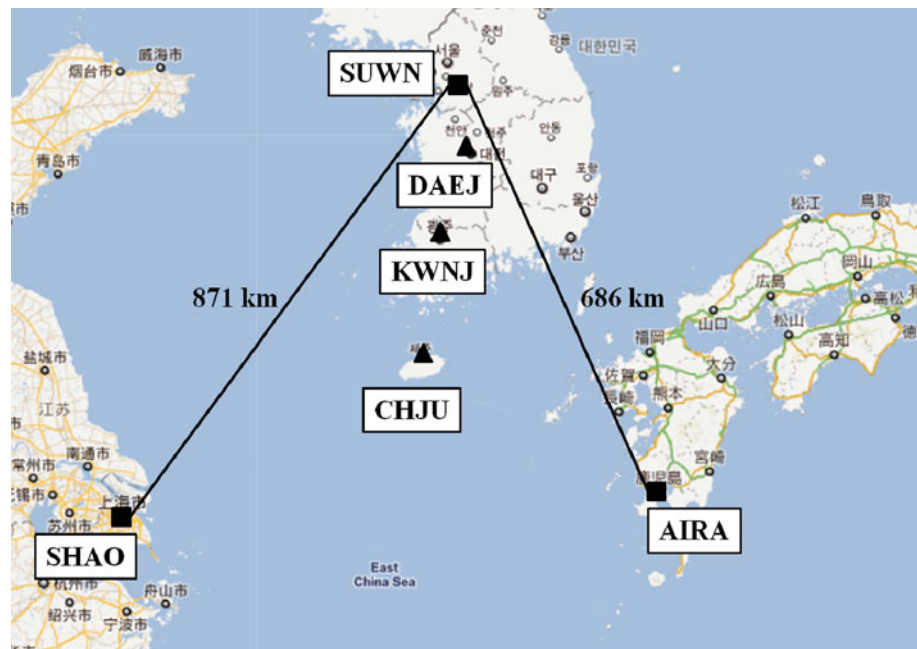


Table 1 Geographic location of the GNSS stations and radiosonde observatories used in the experiments

Name/instrument	Latitude (°)	Longitude (°)	Height (m)
AIRA/GNSS	31.82	130.6	314.66
CHJU/GNSS	33.51	126.53	51.21
DAEJ/GNSS	36.40	127.37	116.83
KWNJ/GNSS	35.17	126.91	71.92
SHAO/GNSS	31.10	121.20	22.03
SUWN/GNSS	37.27	127.05	82.27
Cheju/RS	33.28	126.16	73.0
Kagoshima/RS	31.55	130.55	31.0
Kwangju/RS	35.11	126.81	13.0
Osan/RS	37.10	127.03	52.0
Shanghai/RS	31.40	121.46	4.0

RS Radiosonde

Ultra-rapid ephemeris is not as precise as its orbit counterpart, the satellite clock errors are actually removed by single-differencing the GNSS measurements rather than by using the ephemeris. The satellite orbit is interpolated using the predicted orbit of the IGS Ultra-rapid ephemeris and is fixed during the filtering process.

The IGS tropospheric solution can serve as another reference solution and in fact it can be regarded as performance limit of the real-time PWV solution, taking into account that the IGS ZTD solutions are computed in deferred-time mode using the IGS Final ephemeris.

The international PWV monitor spans from 2010/1/1 through 2010/6/30 and the GNSS data with 30-s spacing were used for real-time data feeding. Accordingly the real-time PWV solutions have the sampling interval of 30 s and

needed to be re-sampled for comparisons with the IGS and RS solutions which have the different sampling interval of 300 s and 12 h, respectively. Note that difference in sampling rate between the GNSS PWV (i.e. RT and IGS) and RS solutions, which is directly related to difference in temporal resolution between the solutions.

Figure 3 shows results obtained with 6-month long PWV monitor for the SUWN–AIRA and SUWN–SHAO links. In Fig. 3a the Real-Time (RT), IGS and Radiosonde (RS) PWV solutions of the AIRA station are plotted together. It should be noted that in the present format of the IGS tropospheric solution, only ZTD (i.e. ZWD + ZHD) is provided instead of ZWD. As a result, ZHD and Π should be given externally to obtain IGS PWV solution and the same values of ZHD and Π used for the RT PWV solution were used again for the IGS PWV solution. As can be seen in Fig. 3a, the RT, IGS and RS solutions generally yield good agreement with each other. The seasonal trend of the PWV is clearly observed in Fig. 3a in the sense that the PWV value becomes greater as time changes from winter to summer, as expected. The agreement between the RT and IGS PWV and RS PWV solutions gets somewhat worse in the summer than in the winter, which is thought to be due to greater temporal and spatial variability of the atmospheric water vapor distribution during summer than that of winter. Results obtained with the SUWN–SHAO link are shown in Fig. 3b and the agreement of the RT and IGS PWV solutions with the RS measurement is generally at the similar level to that of the SUWN–AIRA link. There is a major data gap that spans from 22 through 42 in the Day of Year (DOY) of 2010 and during the gap the GNSS data for several station-days are missing so both RT and IGS PWV solutions are commonly unavailable for this period.

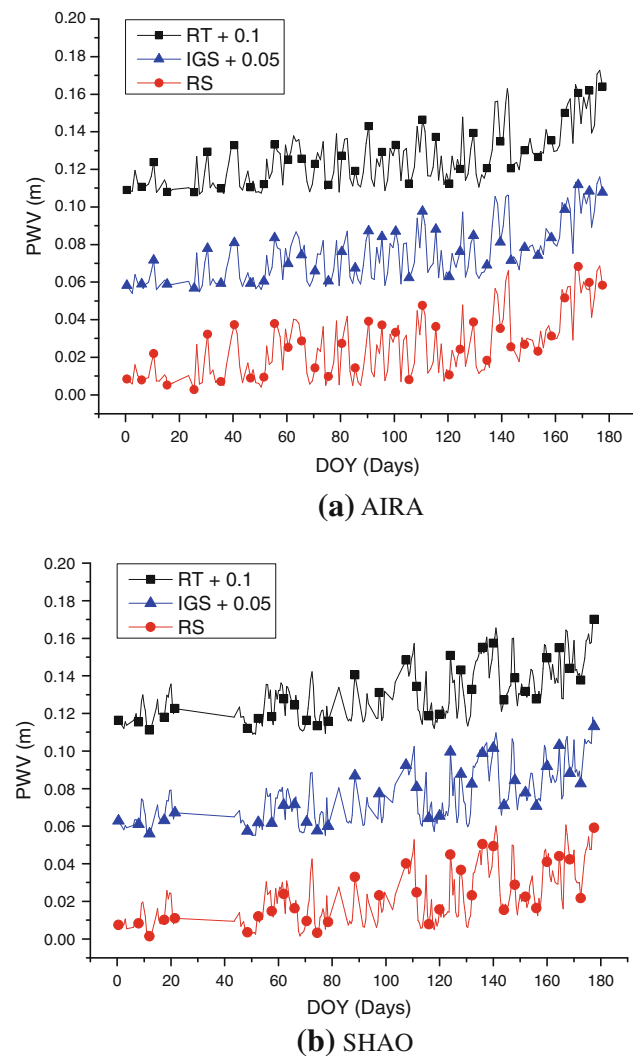


Fig. 3 Results obtained with international PWV network; **a** Real-time (RT), GIPSY OASIS II (IGS) and radiosonde (RS) PWV solutions for the AIRA station in the SUWN–AIRA link. Similar to **a**, **b** shows the RT, IGS and RS PWV solutions for the SHAO station in the SUWN–SHAO link. For a better visibility all the solutions except for RS are plotted with vertical offset. The real-time solution is marked by squares and the IGS and radiosonde solutions are marked by triangles and circles, respectively.

Figure 4 shows the differences between the three PWV solutions, which are RT–RS, RT–IGS and IGS–RS for the SUWN–AIRA and SUWN–SHAO links. The results obtained by comparing between the three PWV solutions are summarized in Table 2 in terms of bias and standard deviation. It can be observed in Fig. 4a that the RT–RS and IGS–RS time series seem somewhat more scattered than RT–IGS in the SUWN–AIRA link. This is mainly because the RT–IGS is the difference between two GNSS-derived PWV solutions and, thus, the RT and IGS solutions are not independent of each other, i.e. intra-technique comparison. Comparing the RT–RS and IGS–RS mutually, the IGS–RS seems more con-

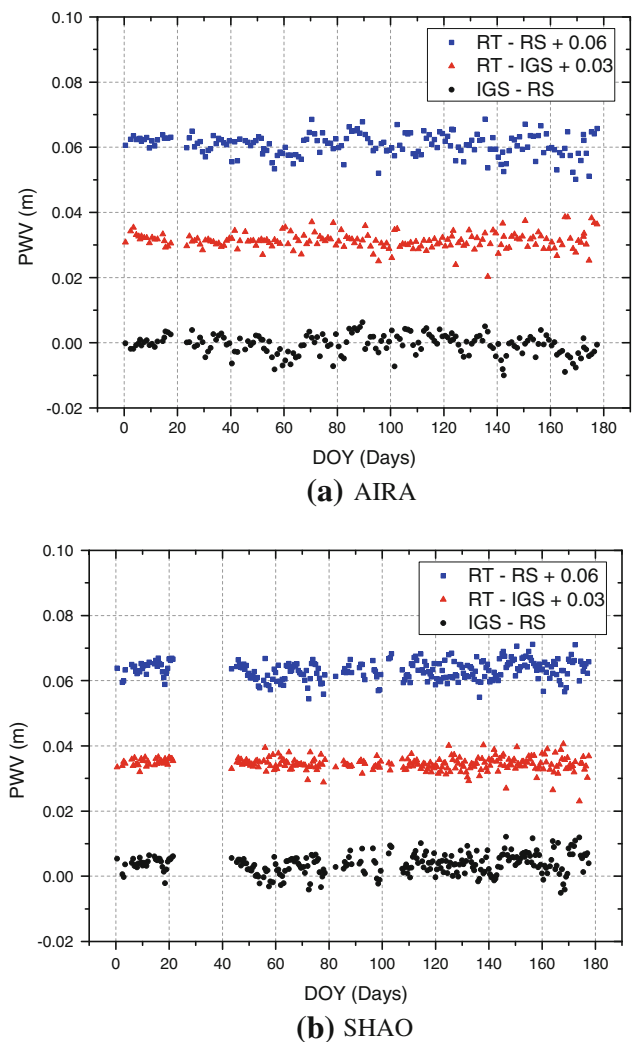


Fig. 4 Differences between the solutions obtained with international PWV network; **a** Differences in solutions between the real-time (RT)–radiosonde (RS), RT–GIPSY OASIS II (IGS) and IGS–RS time series for the AIRA station in the SUWN–AIRA link. Similar to **a**, **b** shows the RT–RS, RT–IGS and IGS–RS PWV time series for the SHAO station in the SUWN–SHAO link. In **a** and **b** the RT–RS and RT–IGS time series are plotted with *vertical offsets* as shown in the legend and RT–RS time series is marked by *squares*, the RT–IGS by *triangles* and the IGS–RS by *circles*

sistent than the RT–RS, especially in DOY 120 through 180, while the scattering of both time series is noticeably low in DOY 1 through 20, which corresponds to winter. There seems to be a systematic trend in the IGS–RS time series and a similar signature can be also observed in RT–RS, although somewhat vague and more difficult to identify in the RT–RS time series. Note that RT–IGS, which is the difference between the same GNSS-derived PWV solutions, does not show such a signature. In Fig. 4b, the differences between the PWV solutions obtained with the SUWN–SHAO link are plotted and compared with Fig. 4a. The three time series in Fig. 4b seem less scattered than their counterparts in Fig. 4a.

Table 2 Differences in PWV between the solutions obtained with international network

Link	RT-RS		IGS-RS		RT-IGS	
	Bias	SD	Bias	SD	Bias	SD
SUWN-AIRA	0.6	3.4	-0.6	3.1	0.3	2.5
SUWN-SHAO	4.8	2.9	3.7	3.1	3.1	2.1

Units in millimeters

Similarly to Fig. 4a, the scattering of the time series is relatively low in the first 20 days of the data span and becomes higher as it approaches the summer.

As can be seen in Table 2, all the solutions agree with each other within 3.4 mm in standard deviation, and comparing difference between the RT and RS with that between the IGS and RS, the IGS solution shows better agreement with the RS solution in the SUWN-AIRA link while the RT solution agrees better with the RS solution in the SUWN-SHAO link. Nontrivial bias was observed in the SUWN-SHAO link, which reaches up 4.8 mm, as shown in the RT-RS column, while bias is kept below 1 mm in the SUWN-AIRA link. The source of the biases shown in the SUWN-SHAO link was not found yet. Based on Table 2, the RMS difference between the three solutions can be computed, and the RMS values of RT-RS, IGS-RS and RT-IGS time series are 3.5, 3.2 and 2.5 mm for the SUWN-AIRA link, respectively, and 5.6, 4.8 and 3.7 mm for the SUWN-SHAO link, respectively. The higher RMS values of the SUWN-SHAO link are due to large biases between the solutions while the standard deviation values obtained with the SUWN-SHAO link are comparable to those obtained with the SUWN-AIRA link.

Timing statistic is one of the important aspects in performance evaluation of real-time systems and the total elapsed time to process 6-month long data was measured for both links, which turned out to be about 9,900 s for the SUWN-AIRA link and 9,700 s for SUWN-SHAO. At this pace, approximately 50 epochs could be processed in 1 s and this is equivalent to say that the data of 50 GNSS stations can be processed in 1 s by the real-time PWV system.

3.2 Domestic PWV monitor

The domestic network is comprised of the four Korean stations whose station designators are SUWN, DAEJ, KWNJ and CHJU. As in the international network, SUWN is configured to the server again. In the proximity of SUWN, there is a meteorological observatory located in Osan. KWNJ happens to have both GNSS and RS stations at the same location. For the CHJU stations, there is an RS observatory close to CHJU. The geographic location of the GNSS stations and RS observatories is summarized in Table 1. The baseline length of the SUWN-DAEJ, SUWN-KWNJ and SUWN-

CHJU links is 101, 233 and 420 km, respectively. Note that no baselines in the domestic network are greater than 500 km. Therefore, the relative PWV estimation was applied for the domestic network. In the relative mode, as discussed before, ZWD of one station needs to be fixed to a priori value, typically that of the server in the server/client structure. In this study the server's ZWD values were imported from the results of the international PWV monitor, being more specific, the ZWD of SUWN from the SUWN-AIRA links. That way the absolutely estimated server's ZWD is fed back to the filter for the relative ZWD estimation of the clients. For the reference solutions in the domestic network, IGS solution was used in the SUWN-DAEJ link and RS solutions in the SUWN-KWNJ and SUWN-CHJU links. This is due to the fact that DAEJ does not have a nearby RS observatory and that the KWNJ and CHJU stations do not belong to the IGS network. The data span of the domestic PWV monitor is the same as that of the international monitor.

Figure 5 shows results obtained with 6-month long domestic PWV monitor. Figure 5a shows the RT solution obtained in the relative mode and IGS PWV solutions for the SUWN-DAEJ link. For comparisons the RT solution obtained in the absolute mode was plotted also. As can be observed in the Fig. 5a, the relative RT solution and the IGS solution yield the similar level of agreement with each other to that obtained in the international network. This shows that the PWV solution can be effectively retrieved in the relative mode for the short baseline cases such as the SUWN-DAEJ link. On the contrary, the RT solution in absolute mode shows clear signature of filter divergence, particularly in the first half of the solution which deviates rapidly from the other solutions soon after the monitor begins.

Figure 5b, c shows the absolute RT, relative RT and RS solutions for the SUWN-KWNJ and SUWN-CHJU links, respectively. Compared with the SUWN-DAEJ link, the absolute RT solution of the two links becomes less and less divergent as the baseline length increases from 101 to 233 and to 420 km. For the SUWN-CHJU link, the relative RT and absolute RT solutions become almost indistinguishable from each other and the standard deviation of differences is computed to be 3.6 mm. Hence either the absolute or relative mode seems to be applicable for the SUWN-CHJU link, although the baseline length is somewhat less than 500 km.

Figure 5d shows differences between the relative RT and reference solutions plotted in Fig. 5a-c, and Table 3 summarizes the bias and standard deviation between the RT and reference solutions obtained with the domestic PWV network. It can be observed from Fig. 5d that difference between the relative RT and reference solutions for the SUWN-DAEJ link seem more consistent and less scattered than those with the SUWN-KWNJ and SUWN-CHJU links. This is again due to the fact that the same GNSS-derived PWV solution is used as the reference solution in the SUWN-DAEJ link, which

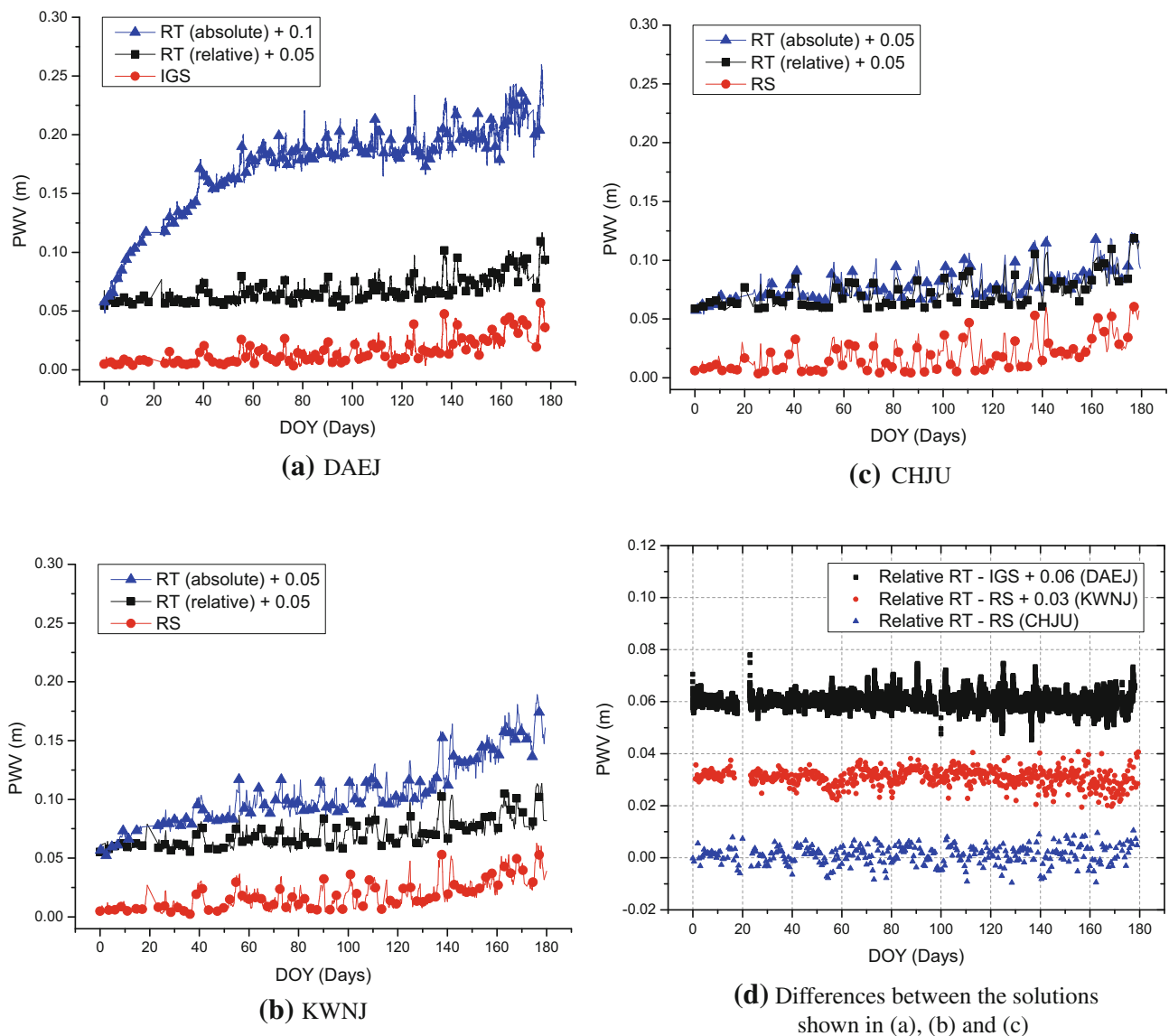


Fig. 5 Results obtained with domestic PWV network: **a** RT solution obtained in the absolute mode, the RT in the relative mode and the GPSY OASIS II (IGS) solutions for the DAEJ station in the SUWN–DAEJ link. Likewise, **b** and **c** show the absolute RT, relative RT and RS PWV solutions for the KWNJ and CHJU stations, respectively. The

absolute and relative RT solutions are vertically shifted and aligned for a better visibility. **d** Differences in PWV between the relative RT and the reference solutions shown in **a–c**, i.e. the IGS solution for DAEJ and RS for KWNJ and CHJU

renders the comparison to be intra-technique rather than inter-technique, while radiosonde measurements are compared with the RT solutions in the other links. The standard deviation of differences between the relative RT and the IGS solutions in the SUWN–DAEJ link is computed to 2.5 mm, which is at the same level of agreement as that obtained with the international network. The standard deviation of the relative RT–RS time series in the SUWN–KWNJ and SUWN–CHJU links is computed to be 3.3 and 3.6 mm, respectively.

As can be seen in Table 3 the standard deviation of difference between the relative RT and reference solutions ranges from 2.5 to 3.6 mm. This level of agreement is almost the

same as that obtained with the international network, which suggests that the relative PWV estimation is effective in remedying a specific type of filter divergence that typically happens to densely distributed or regional GNSS PWV networks where member stations are not separated from each other sufficiently. The RMS values of solution differences are computed to be 2.7, 3.5 and 4.3 mm for the SUWN–DAEJ, SUWN–KWNJ and SUWN–CHJU links, respectively.

Compared with the results reported by Bevis et al. (1992) and Rocken et al. (1997), the level of agreement between the RT PWV and RS solutions in Tables 2 and 3 seems somewhat higher—approximately 0.5–1.4 mm in terms of column

Table 3 Differences in PWV between the relative RT and reference solutions obtained with domestic network

Link	Relative RT–RS		Relative RT–IGS	
	Bias	SD	Bias	SD
SUWN-DAEJ	–	–	1.1	2.5
SUWN-KWNJ	1.2	3.3	–	–
SUWN-CHJU	2.4	3.6	–	–

Units in millimeters

water which is translated to 3.3–9.3 mm in range measurements. Such discrepancy in performance may be attributed to several sources. A major part of the difference between the RT and RS solutions seems to come from different conditions in performance evaluation between the previous works and our own. More specifically, comparisons between different types of PWV solutions generally become more inconsistent for stations in coastal areas than those in the interior of the continents and, for the same station, more inconsistent in the summer than in the winter. Different levels of variability (both spatially and temporally) of the atmospheric water vapor can account for these tendencies.

As evidence supporting this view, the standard deviation was found to be improved by limiting the duration of comparison to the first 20 days of the entire data span, both with international and domestic networks. Specifically, the value of standard deviation of the RT–RS was reduced to 1.5 mm for the SUWN–AIRA link and 2.1 mm for the SUWN–SHAO station by limiting the duration of comparison, which is comparable to those reported by [Bevis et al. \(1992\)](#), [Rocken et al. \(1997\)](#), and [Karabatic et al. \(2011\)](#). Also, the standard deviations of the SUWN–DAEJ, SUWN–KWNJ and SUWN–CHJU links were reduced to 1.4, 1.5 and 2.9 mm, respectively.

Another source of discrepancy in performance between these previous works and our own is that the atmospheric temperature and surface pressure used in computing the RT PWV solution were not actually measured as was done in the previous works but calculated from a simple model. It is noted that the agreement between two reference solutions—the IGS and RS solutions—is slightly greater than 3 mm in standard deviation and is also worse than the results of [Bevis et al. \(1992\)](#) and [Rocken et al. \(1997\)](#). The use of the in situ measurement of the temperature and pressure of the individual stations would enhance the accuracy of the hydrostatic delay as well as the conversion factor (Eq. 5) used in the RT and IGS solutions. However, this requires additional meteorological sensors and data transfer setup and was not considered in the study.

Finally, as far as the comparison between the RT and IGS solutions is concerned, another possible source of solution discrepancy is so-called the “processing effect” ([Teke et al.](#)

[2011](#)) where GNSS-derived PWV solutions can differ from each other by a few millimeters in ZTD depending on which software is used, even though the same GNSS data are used.

4 Conclusions

Performance of the real-time GNSS PWV monitoring system was evaluated by conducting international and domestic PWV monitoring. Based on 6-month long continuous PWV monitor, the real-time PWV solution was found to agree with the radiosonde measurements and the IGS deferred-time solutions at the range of 2.1–3.4 mm in standard deviation for the international network and 2.5–3.6 mm for the domestic network. Further improvements in performance may be attempted using in-situ observation of pressure and temperature of the individual stations.

It should be noted that the requirement of fixing the server’s ZWD in relative PWV estimation is not difficult to meet in real-time. One way to achieve this is to include in a network at least one client station that is sufficiently separated by the server. That way every time new data are transferred to the server, the server performs first the absolute PWV estimation with the client. After obtaining the server’s ZWD value in the absolute mode, the ZWD value of the server can be used in the relative PWV estimation sessions that are performed subsequently with the other clients in the network. Recalling that the SUWN–CHJU link can be processed either in absolute or relative mode, the domestic network would be configured to be self-sufficient, that is, by processing the SUWN–CHJU link first in the absolute mode and the other links in the relative mode, which would make it unnecessary to import the server’s ZWD values externally.

Acknowledgments The authors would like to thank the editor, associate editor and four anonymous reviewers for providing constructive suggestions and helpful comments to improve the manuscript. This research was supported by the Korea Meteorological Administration R&D program under Grant CATER 2012-6150.

References

- Bar-Server YE, Kroger PM, Borjesson JA (1998) Estimating horizontal gradients of tropospheric path delay with a single GPS receiver. *J Geophys Res* 103(B3):5019–5035
- Bevis M, Businger S, Herring T, Rocken C, Anthes R, Ware R (1992) GPS meteorology: remote sensing of atmospheric water vapor using GPS. *J Geophys Res* 97:15787–15801
- Böhm J, Niell A, Tregoning P, Schuh H (2006) Global mapping function (GMF): a new empirical mapping function based on numerical weather model data. *Geophys Res Lett* 33:L07304. doi:10.1029/2005GL025546
- Brown RG, Hwang PYC (1997) Introduction to random signals and applied Kalman filtering, 3rd edn. Wiley, New York

- Byram S, Hackman C, Tracey J (2011) Computation of a high-precision GPS-based troposphere product by the USNO. *Proc ION GNSS 2011*:572–578
- Byram S, Hackman C (2012) Computation of the IGS final troposphere product by the USNO (2012) IGS workshop, Olstzyn
- Byun S, Bar-Server Y (2009) A new type of troposphere zenith path delay product of the international GNSS service. *J Geod* 83(3–4):1–7
- de Haan S, Barlag SJM (2002) Amending numerical weather prediction forecasts using GPS integrated water vapour: a case study COST action 716 workshop: exploitation of ground-based GPS for meteorology
- Elgered G, Plag HP, Van der Marel H, Barlag S, Nash J (2005) COST action 716—exploitation of ground-based GPS for operational numerical weather prediction and climate applications. Official Publications of the European Communities, Luxembourg
- Gendt G, Dick G, Reigber C, Tomassini M, Liu Y, Ramatschi M (2004) Near real-time GPS water vapor monitoring for numerical weather prediction in Germany. *J Meteorol Soc Japan Ser II* 82:361–370
- Gutman SI, Sahn SR, Benjamin SG, Schwartz BE, Holub K, Stewart JQ, Smith TL (2004) Rapid retrieval and assimilation of ground based GPS precipitable water observations at the NOAA forecast systems laboratory: impact on weather forecasts. *J Meteorol Soc Jpn* 82(1B):351–360
- Heise S, Dick G, Gendt G, Schmidt T, Wickert J (2009) Integrated water vapor from IGS ground-based GPS observations: initial results from a global 5-min data set. *Ann Geophys* 27:2851–2859. doi:[10.5194/angeo-27-2851-2009](https://doi.org/10.5194/angeo-27-2851-2009)
- Hernandez-Pajares M, Juan JM, Sanz J, Colombo OL, Van Der Marel H (2001) A new strategy for real-time integrated water vapor determination in WADGPS networks. *Geophys Res Lett* 28(17):3267–3270
- Iwabuchi T, Rocken C, Lukes Z, Mervart L, Johnson J, Kanzaki M (2006) PPP and network true real-time 30 sec estimation of ZTD in dense and giant regional GPS network and the application of ZTD for nowcasting of heavy rainfall. In: Proceedings of the Institute of Navigation, 19th international technical meeting of the Satellite Division, ION GNSS 2006, vol. 4, pp 1902–1909
- Iwabuchi T, Rocken C, Wada A, Kanzaki M (2011) True real-time slant tropospheric delay monitoring system with site dependent multipath filtering. In: 24th International technical meeting of the Satellite Division of the Institute of Navigation 2011, ION GNSS 2011, vol 1, pp 579–587
- Karabatic A, Weber R, Haiden T (2011) Near real-time estimation of tropospheric water vapour content from ground based GNSS data and its potential contribution to weather now-casting in Austria. *Adv Space Res* 47:1691–1703
- Kouba J (2008) Implementation and testing of the gridded Vienna Mapping Function 1 (VMF1). *J Geod* 82(4–5):193–205
- Lee S, Schutz B, Lee C, Yang S (2008) A study on the common-view and all-in-view GPS time transfer using carrier-phase measurements. *Metrologia* 45:156–167
- Lee S, Kim J (2009) Performance evaluation of real-time carrier-phase GPS time transfer. *Meas Sci Technol* 20:065105
- Rocken C, Van Hove T, Ware R (1997) Near real-time sensing of atmospheric water vapor. *Geophys Res Lett* 24:3221–3224
- Saastamoinen J (1972) Atmospheric correction for the troposphere and stratosphere in radio ranging of satellites. The use of artificial satellites for geodesy. *Geophys Monogr Ser, Amer Geophys Union* 15:247–251
- Schueler T, Hein GW, Eissfeller B (2000) Towards an optimal strategy for GPS wet delay Kalman filtering. In: Proceedings of the IAIN World Congress and the 56th annual meeting of the Institute of Navigation, San Diego, pp 762–771
- Stevens M (1999) Optimal climate signal detection in four dimensions. *J Geophys Res* 104:4089–4099
- Teke K, Böhm J, Nilsson T, Schuh H, Steigenberger P, Dach R, Heinkelmann R, Willis P, Hass R, Espada S, Hobiger T, Ichikawa R, Shimizu S (2011) Multi-technique comparison of troposphere zenith delays and gradients during CONT08. *J Geod* 85:395–413
- Ware RH, Fulker DW, Stein SA, Anderson DN, Avery SK, Clark RD, Drogemeier KK, Kuettner JP, Minster JB, Sorooshian S (2000) SuomiNet: a real-time national GPS network for atmospheric research and education. *Bull Am Meteorol Soc* 81:677–694